THE JOURNAL OF PHYSICAL CHEMISTRY LETTERS
A JOURNAL OF THE AMERICAN CHEMICAL SOCIETY

pubs.acs.org/JPCL
Letter

Insights into PSII's $S_3Y_Z^{\bullet}$ State: An Electronic and Magnetic Analysis

Felix Rummel, Thomas Malcomson,* Maxim Barchenko, and Patrick J. O'Malley

Cite This: J. Phys. Chem. Lett. 2024, 15, 499−506
Read Online
ACCESS | Metrics & More | Article Recommendations | Supporting Information

ABSTRACT: Using BS-DFT (broken-symmetry density functional theory), the electronic and magnetic properties of the $S_3Y_Z^{\bullet}$ state of photosystem II were investigated and compared to those of the S_3 state. While the O5 oxo−O6 hydroxo species presents little difference between the two states, a previously identified $[O5O6]^{3-}$ exhibits reduced stabilization of the O5−O6 shared spin. This species is shown to have some coupling with the $Y_Z^{\bullet}$ center through Mn_1 and O6. Similarly, a peroxo species is found to exhibit significant exchange couplings between the $Y_Z^{\bullet}$ center and the Mn cluster through Mn_1. Mechanistic changes in O−O bond formation in $S_3Y_Z^{\bullet}$ are highlighted by analysis of IBOs (intrinsic bonding orbitals) showing deviation for Mn_1 and O6 centered IBOs. This change in coupling interactions throughout the complex as a result of $S_3Y_Z^{\bullet}$ formation presents implications for the determination of the mechanism spanning the end of the S_3 and the start of the S_4 states, affecting both electron movement and oxygen bond formation.

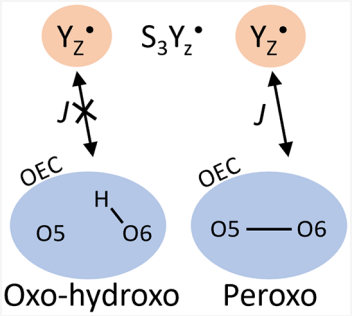

Water oxidation, and subsequent dioxygen formation, is catalyzed by the manganese−calcium oxygen-evolving complex (OEC) held within the photosystem II protein framework.[1−4] Taking place over a series of steps such that

$$2H_2O \xrightarrow{4h\nu} O_2 + 4e^- + 4H^+ \quad (1)$$

the mechanism can effectively be broken down into a series of photoactivated oxidation and deprotonation steps with modern efforts, both experimental and theoretical, directed toward the determination of both the order and relative timing of each event.[5−13] An in-depth understanding of this catalytic cycle is intrinsic in driving the development of future technologies aimed at harnessing both the water-splitting potential of the complex and its capacity to store energy to account for an increasing global energy demand.[14−20]

During water oxidation, the OEC moves through five states (S_0 to S_4) determined by the number of oxidizing equivalents stored, signified by the subscript numeral. Of these states, S_0−S_3 can be isolated for study, while S_4 has yet to be isolated and is strongly assumed to be transient. Due to the transient nature of S_4, increased importance is then placed on the description of S_3 in order to both understand S_3 itself and determine viable structures at the beginning of S_4.

Early crystal structures of the S_3 state[21,22] show a short (≈1.5 Å) O−O distance between O5 and O6 (Figure S1) suggesting early onset O−O bond formation in the form of a peroxide or superoxide structure.[22] However, this idea is excluded when interpreted alongside earlier spectroscopic[23,24] and later SFX structures,[25,26] suggesting an O5−O6 distance of ≈2.0 Å and therefore noninteracting or weakly interacting oxygens at the O5 and O6 positions. Recent theoretical work has put forward a comprehensive overview of the potential energy surface as a function of O5−O6 distance throughout the S_3 state.[5−8] An oxo−hydroxo O5−O6 formation was presented, in line with previous work in the field,[24,27−30] transitioning to an oxo−oxyl intermediate close to the geometry of modern crystal structures.[9] Finally, this proceeds to a peroxo structure as O5−O6 distance is reduced.

In addition to the initial bonding interaction between O5 and O6, the transition from S_3 to S_4 also comprises a final oxidation event,[31−35] during which the local Tyr161 (Y_Z) is oxidized to a $Y_Z^{\bullet}$ state. This oxidation is proposed to have occurred within 50 μs after the flash. This is thought to be followed by a deprotonation event with the proton leaving through the Cl1 channel (200−500 μs). This is followed by OEC oxidation (500−1200 μs), $Y_Z^{\bullet}$ reduction (500−730 μs), and molecular oxygen formation (≈1200 μs).[34,35] The oxidization event can, in turn, be considered in three discrete phases:[36] First, there is the oxidation of Y_Z. This is followed by an extended lag phase during which additional oxidation is not reported. Finally, the resulting $Y_Z^{\bullet}$ is reduced. This is followed by the release of molecular oxygen and subsequently another water molecule being inserted and deprotonated along with the reformation of the S_0 state.

Since the initiation of this final oxidation step is thought to mark the formal transition between the S_3 and S_4 states, and the subsequent release of the dioxygen molecule, deducing the effect of Y_Z reduction on the overall S_3 PES is a vital step in understanding the transition from a oxo−hydroxo O5−O6

Received: October 29, 2023
Revised: December 27, 2023
Accepted: January 2, 2024
Published: January 8, 2024

https://doi.org/10.1021/acs.jpclett.3c03026
J. Phys. Chem. Lett. 2024, 15, 499−506

formation to the pre-O_2 species. In continuation of previously conducted work,[5] and accounting for the findings put forward by Pushkar et al.[37] suggesting that the formation of the oxyl may occur during the lag phase, after the oxidation of Y_Z, but prior to its eventual reduction, we present an investigative comparison of the O5−O6 bond formation potential energy surface both before and after the oxidation of Y_Z in an attempt to better understand how the presence of this local $Y_Z^\bullet$ radical species influences the activity of the OEC and the potential role that $Y_Z^\bullet$ formation has on influencing the O−O species formed at each stage of the S_3 state.

In the $S_3Y_Z^\bullet$ state the Y_Z-161 residue is a positive radical, resulting in the presence of an additional unpaired spin center, increasing the total number of possible broken-symmetry (BS) states. It was found that, in order to produce the correct BS solutions in this state, with $Y_Z^\bullet$ allocated a β spin, intuitively flipping the spin on either the C1 or oxygen atom of the $Y_Z^\bullet$ residue proved to be insufficient, instead requiring both atoms be flipped or indeed all carbon atoms in the $Y_Z^\bullet$ ring as well as the oxygen (see Figure 1). Flipping just C1 (see Figure 1)

A

Flipped centres	Total Mulliken spin Y_Z	[O5O6]	E_{HS}-E_{BS} kcal mol^{-1}
O	1.01	-0.59	16.7
O, C1	-0.92	1.16	0.1
O, Y_Z ring C	-0.92	1.16	0.1

B

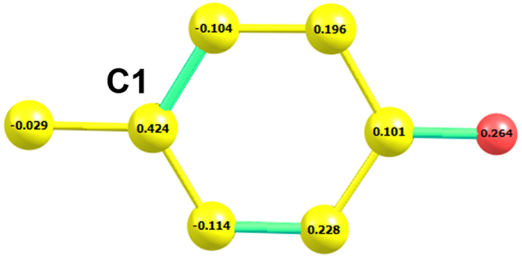

Figure 1. Taken from a high-spin O5−O6 = 2.1 Å model. (A) Total calculated Mulliken spin population for the Y_Z residue for different BS "flipspin" inputs, as well as the relative energies compared to the high-spin system. (B) Mulliken spin populations of the $Y_Z^\bullet$ residue. Yellow: carbon. Red: oxygen. Hydrogens are omitted for clarity.

which carries a majority of the unpaired spin led to problems in the convergence of the wave function for many BS states, as such data for comparison with Figure 1A could not be obtained. Similarly flipping just the $Y_Z^\bullet$ oxygen yielded the incorrect Mulliken spin distribution, with the $Y_Z^\bullet$ remaining in the high-spin state. Instead the spin shared between O5 and O6 was found to be flipped. As a result of this, any BS state calculated with the incorrect spin flips will not produce the desired spin distribution and as such will compromise both the resulting BS energy and the calculated exchange couplings between spin centers.

In the S_3 state the Y_Z residue was found to be protonated and hydrogen bonded to its hydrogen bonding partner His190, whereas upon generation of the $S_3Y_Z^\bullet$ state the proton from the $Y_Z^\bullet$ residue moved onto the His190 residue, leaving the $Y_Z^\bullet$ oxygen deprotonated. It was found that this movement occurred spontaneously and optimization with the proton on either $Y_Z^\bullet$ or His190 resulted in the same geometry, with His190 bearing the proton, leaving the $Y_Z^\bullet$ oxygen as a deprotonated phenoxyl. This suggests barrier-less proton transfer or a negligible barrier for proton movement upon oxidation, rather than a separate discrete proton transfer event. Models with O5 and O6 in a peroxo or oxo−oxo arrangement (r[O5O6] = 1.4 or 2.4 Å respectively) were created with the proton fixed on Y_Z or His190 to investigate the energy difference for various BS states as well as the HS (high-spin) state. It was found that the peroxo-like arrangement structures with the proton fixed on Y_Z were on average 22 kcal mol^{-1} higher in energy than the His protonated counterpart. In the oxo−oxo arrangement, this was increased to 26 kcal mol^{-1}. The $Y_Z^\bullet$ residue remains hydrogen bonded through the phenoxyl oxygen to the OEC through the calcium bound W4; this was not observed to change the position or bonding nature significantly when the protonation state of the Y_Z residue changed. Similarly the Y_Z residue can also hydrogen bond through a nearby water molecule indirectly to the OEC by several pathways depending on proton orientation, but again the position and orientation of this water molecule was also unaffected by the protonation state.

Previous work in the S_3 state investigated several potential energy surfaces (PESs) resulting in the identification of three key species:[5] an O5 oxo−O6 hydroxo; a $[O5O6]^{3-}$ with a single unpaired β spin shared between O5 and O6; and a peroxo species with a formal bond between O5 and O6. Once the Y_Z residue is oxidized and the $S_3Y_Z^\bullet$ state formed there is an additional spin center present. For the O5 oxo−O6 hydroxo there are now 5 spin centers (Mn_1−Mn_4 and Y_Z) yielding 15 unique BS states (and 1 HS state), whereas in the S_3 state, there are only 7 unique BS states. The relative energies of these are compared in Figure 2. The most stable BS states are either

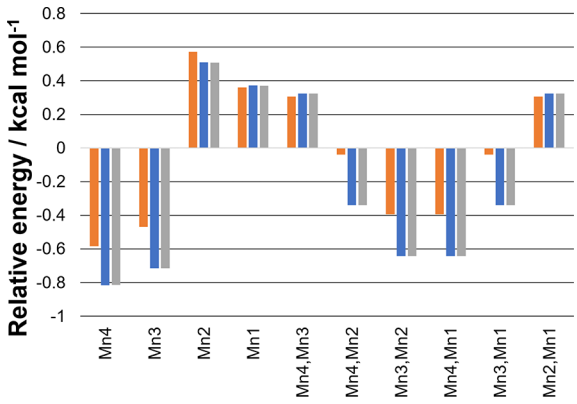

Figure 2. Relative energy of the BS states to the HS state for the oxo−hydroxo models: more negative values correspond to more stable BS states. The "flipped" centers are indicated. Orange: S_3 state. Blue: $S_3Y_Z^\bullet$ state with $Y_Z^\bullet$ as α. Gray: $S_3Y_Z^\bullet$ state with $Y_Z^\bullet$ as β.

with Mn_4 or Mn_3 antiparallel to all other spin centers regardless of the $Y_Z^\bullet$ spin alignment or whether the model is in the S_3 state or $S_3Y_Z^\bullet$ state. Furthermore, the alignment of the $Y_Z^\bullet$ radical has no significant effect on the BS energies in the $S_3Y_Z^\bullet$ state. This, in turn, suggests a lack of, or weak coupling between, the $Y_Z^\bullet$ radical and the Mn cluster; this aligns with previous work by Retegan et al.[38] in which the $S_2Y_Z^\bullet$ showed no coupling between the $Y_Z^\bullet$ residue and the OEC.

The lack of coupling of the oxo−hydroxo OEC with the nearby $Y_Z^\bullet$ radical observed in Figure 2 is reflected in the calculated J values shown in Table 1. Comparing the S_3 and

https://doi.org/10.1021/acs.jpclett.3c03026
J. Phys. Chem. Lett. 2024, 15, 499−506

Table 1. BS-DFT Calculated Mn−Mn, Mn−Y_Z, Mn−O, and O−$Y_Z^{\bullet}$ Exchange Couplings, J Values Obtained for the O5 Oxo−O6 Hydroxo, the Broad Minima Corresponding to $[O5O6]^{3-}$ and the O5−O6 Peroxo State, in Both the S_3 and $S_3Y_Z^{\bullet}$ State[a]

	oxo−hydroxo		$[O5O6]^{3-}$		peroxo	
	$S_3Y_Z^{\bullet}$	S_3	$S_3Y_Z^{\bullet}$	S_3	$S_3Y_Z^{\bullet}$	S_3
J_{43}	−35.6	−26.1	−7.7	−17.8	21.4	17.8
J_{42}	0.6	0.4	−0.6	0.6	1.8	1.2
J_{41}	3.7	3.2	−39.6	−87.7	−3.7	−5.8
$J_{4-O5/O6}$			−536.9	−1051.7		
J_{4Y_Z}	0.0		−4.1		−10.1	
J_{32}	8.3	9.4	17.5	11.3	11.1	10.1
J_{31}	−0.1	−1.4	−12.8	−25.7	−4.2	−6.7
$J_{3-O5/O6}$			−342.1	−432.8		
J_{3Y_Z}	0.0		−3.9		4.9	
J_{21}	10.6	12.0	12.6	14.1	−30.8	−33.5
$J_{2-O5/O6}$			0.5	3−0.2		
J_{2Y_Z}	0.0		0.0		−11.1	
$J_{1-O5/O6}$			−849.9	−1301.1		
J_{1Y_Z}	0.0		1.3		−27.6	
$J_{O5/O6-Y_Z}$			−16.4			

[a]All values are in cm^{-1}.

$S_3Y_Z^{\bullet}$ J values, it can be seen that the magnitude is similar for all Mn−Mn couplings. There is also an apparent lack of significant coupling between the Mn centers and the $Y_Z^{\bullet}$ residue, and the coupling here is several orders of magnitude smaller. This agrees with previous findings by Retegan et al.[38] who reported a similar difference in magnitude for the $S_2Y_Z^{\bullet}$ state.[38] The dominant antiferromagnetic coupling between Mn_3 and Mn_4 agrees well with the BS4 and BS3 states being the most stable.

During O5−O6 bond formation it is necessary to deprotonate O6. At a large O5−O6 separation (>2.2 Å) this yields an oxo−oxo species while optimization at a short O5−O6 distance (<1.6 Å) yields a peroxo structure with O5 and O6 bonded. Optimization at around 2 Å yields a $[O5O6]^{3-}$ species both in the S_3 and $S_3Y_Z^{\bullet}$ state. In both states an unpaired β electron is shared between O5 and O6 while other spin centers are in an α alignment; a spin density plot for the $S_3Y_Z^{\bullet}$ state is shown in Figure S3 and illustrates both this and the delocalization of the radical throughout the $Y_Z^{\bullet}$ residue.

The BS-DFT energies for the $[O5O6]^{3-}$ species are shown in Figure 3 where for any given BS state the stabilization is reduced in the $S_3Y_Z^{\bullet}$ state in contrast to the increased stabilization observed in the oxo−hydroxo geometry (Figure 2). Interestingly, the spin alignment of the $Y_Z^{\bullet}$ as for the O5 oxo−O6 hydroxo has no obvious effect on the energies of most BS states. However, very small differences can be observed for some states, such as the BS1 state. The most stable BS state for both S states is an antiparallel alignment of the [O5O6] shared spin to all other spin centers as expected given the relative magnitudes of the Mn−$O_{5/6}$ J couplings compared to the Mn−Mn and Y_Z−$O_{5/6}$ J couplings (Table 1). Given the relative magnitudes of the [O5O6] couplings, this strongly marked effect may overshadow the more subtle remaining couplings throughout the system.

The $[O5O6]^{3-}$ HS form with the shared spin between the oxygens antiparallel is energetically the most favored (see

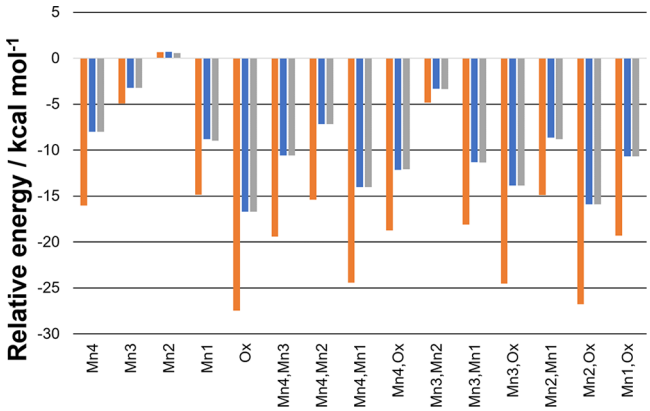

Figure 3. Relative energy of the BS states to the HS state for the $[O5O6]^{3-}$ species; more negative values correspond to more stable BS states. The "flipped" centers are indicated. Orange: S_3 state. Blue: $S_3Y_Z^{\bullet}$ state with $Y_Z^{\bullet}$ as α. Gray: $S_3Y_Z^{\bullet}$ state with $Y_Z^{\bullet}$ as β.

Table S1); it is also clear from Table 1 that it is the Mn−O5/O6 couplings which dominate the spin interactions. As such, the relative reduced stability of the $[O5O6]^{3-}$ species in the $S_3Y_Z^{\bullet}$ state could be rationalized by the decreased stabilization of the shared spin by the Mn centers. Furthermore, in the $S_3Y_Z^{\bullet}$ state, coupling between the $Y_Z^{\bullet}$ spin and the OEC is observed, particularly between the shared oxygen spin and $Y_Z^{\bullet}$ (see Table 1). From Table 1 it can be seen that in both states the spin shared between O5 and O6 is stabilized by strong antiferromagnetic coupling with the Mn_1, Mn_3, and Mn_4 centers. These couplings are significantly larger than all other couplings and so rationalize why this center dominates the BS energies. In contrast, the coupling between Mn_2 and O5 and O6 is negligible. This is likely due to the fact that O5 and O6 are directly bonded to Mn_1, Mn_3, and Mn_4 but not to Mn_2, therefore preventing the strong coupling observed with the other metal centers. This observation is further backed up by the low coupling between Mn_2 and Mn_4 when compared to stronger coupling with Mn_1 and Mn_3. This stabilizing coupling with the Mn ions is somewhat diminished in the $S_3Y_Z^{\bullet}$ state compared to the S_3 state with Mn−[O5O6] couplings decreasing on average by a factor of 1.6, rationalizing why the BS-DFT energies in Figure 3 are reduced in the $S_3Y_Z^{\bullet}$ state. Interestingly, some antiferromagnetic coupling is also observed between $[O5O6]^{3-}$ and the $Y_Z^{\bullet}$ radical comparable in magnitude to the Mn−Mn couplings, showing the presence of couplings between the OEC and the Y_Z residue. Similarly, although weaker, the Mn ions also show coupling with the $Y_Z^{\bullet}$ spin. Comparing the S_3 and $S_3Y_Z^{\bullet}$ state, the most significant changes in magnitude are observed for couplings involving Mn_1 and O5/O6.

At short O5−O6 separation the OEC optimized to a peroxo type structure, with a formal O−O bond between O5 and O6. For this species, the BS1 state was found to be the lowest in energy. This peroxo geometry shows a much more significant coupling between the OEC and the $Y_Z^{\bullet}$ radical. The calculated J values for the peroxo species both in the S_3 and $S_3Y_Z^{\bullet}$ state are shown in Table 1 and the BS energies in Figure 4. While the Mn−Mn couplings are very similar for the S_3 and $S_3Y_Z^{\bullet}$ state, significant coupling between the Mn centers and the $Y_Z^{\bullet}$ radical are observed, the effect of which is reflected in the BS energies, despite the comparatively large separation of the OEC and the $Y_Z^{\bullet}$ radical. The $Y_Z^{\bullet}$ radical shows antiferromagnetic coupling with Mn_4, Mn_2, and Mn_1 and shows weak ferromagnetic

https://doi.org/10.1021/acs.jpclett.3c03026
J. Phys. Chem. Lett. 2024, 15, 499−506

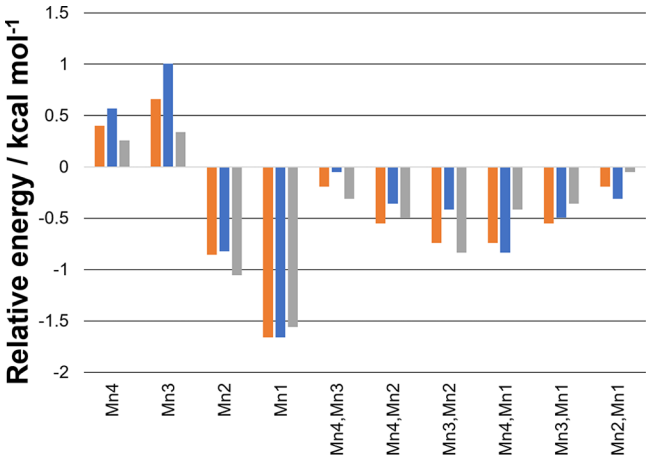

Figure 4. Relative energy of the BS states to the HS state for the peroxo species: more negative values correspond to more stable BS states. The "flipped" centers are indicated. Orange: S_3 state. Blue: $S_3Y_Z^{\bullet}$ state with $Y_Z^{\bullet}$ as α. Gray: $S_3Y_Z^{\bullet}$ state with $Y_Z^{\bullet}$ as β.

coupling with Mn_3, with the strongest coupling observed with the Mn_1 center. Mn_3 is shielded from $Y_Z^{\bullet}$ by Mn_2 and Ca^{2+} rationalizing the weaker coupling. The BS energies indicate the most stable BS state to be BS1 with all other centers antiparallel to it. This agrees well with the strong antiferromagnetic Mn_1–$Y_Z^{\bullet}$ coupling and indeed Mn_1–Mn_2.

Investigating the electronic changes by analysis of the intrinsic bonding orbitals (IBOs) in the $S_3Y_Z^{\bullet}$ state for the partial O–O bond formation of the $[O5O6]^{3-}$ shows no major differences between the S_3 and $S_3Y_Z^{\bullet}$ state for the high-spin M_s = 6.5 oxo–oxo/peroxo surface, see Supporting Information Figures S4 and S5. Here the only apparent difference is the π bonding lone pair on O6 (magenta) for which the spin orbital's orientation differs; in the S_3 state, the spin orbital lies along the Mn_1–O6–Mn_3 plane, whereas in the $S_3Y_Z^{\bullet}$ state it is perpendicular to it.

For the BS1 oxo–oxo/peroxo surface (M_s = 3.5) (Figure 5), 5 IBOs were observed to change significantly across the PES, as opposed to only four in the S_3 state (see Figure S6). An α electron from the lone pair on O6 (green) that shows some π bonding character to Mn_1 forms the α component of the O5–O6 bond around 2 Å. Also, an α electron from a Mn_4–O5 σ bond (blue) moves to Mn_4 around 2 Å, while the corresponding β electron from the Mn_4–O5 σ bond (red) moves to form the β component of the O5–O6 bond around 1.8 Å. These three IBOs and their changes are the same for both the S_3 and the $S_3Y_Z^{\bullet}$ state. However, the remaining two IBOs differ: In the S_3 state a β electron from a Mn_1–O6 σ bond moved onto Mn_1 around 1.8 Å with an associated orbital change of 1 e^{-1} (see Figure S6), whereas here, in the $S_3Y_Z^{\bullet}$ state, the β electron from a Mn_1–O6 σ bond (yellow) moves to become a lone pair β on O6 around 1.8 Å with an associated orbital change of 0.5 e^{-1} (see Figure S7). Finally, a lone pair β electron (magenta), which shows no interaction with Mn_1 initially, unlike the corresponding α electron (green), moves to Mn_1 around 1.8 Å with an associated orbital change of 1.5 e^{-1}. These two changes still amount to an overall change of 1 e^{-1} going toward Mn_1 but present different sources for the observed change.

While at first glance a long-range spin–spin interaction such as the coupling between the OEC and the $Y_Z^{\bullet}$ residue seems unlikely, long-range spin–spin couplings are well established in the literature for both organic and metallic spin centers.[39−42] Within the OEC, the spin–spin couplings have been shown to be superexchange type interactions,[43] relying on the oxygen bridges between Mn ions. While superexchange through space is possible, in examples studied by Stanford et al.[41] it was shown that favorable orbital overlap is required; it has also been shown that long-range superexchange can exist in certain systems containing two spin centers linked by covalent bonds.[42] Additionally, solvent molecules may mediate coupling interactions between spin centers and can aid in electron transfer mechanisms.[44−46] Liu et al.[40] demonstrated the presence of long-range coupling between two spin centers, linked by a flexible linker which did not allow for delocalization, and showed that increasing linker length did not always have an effect on the magnitude of the spin–spin

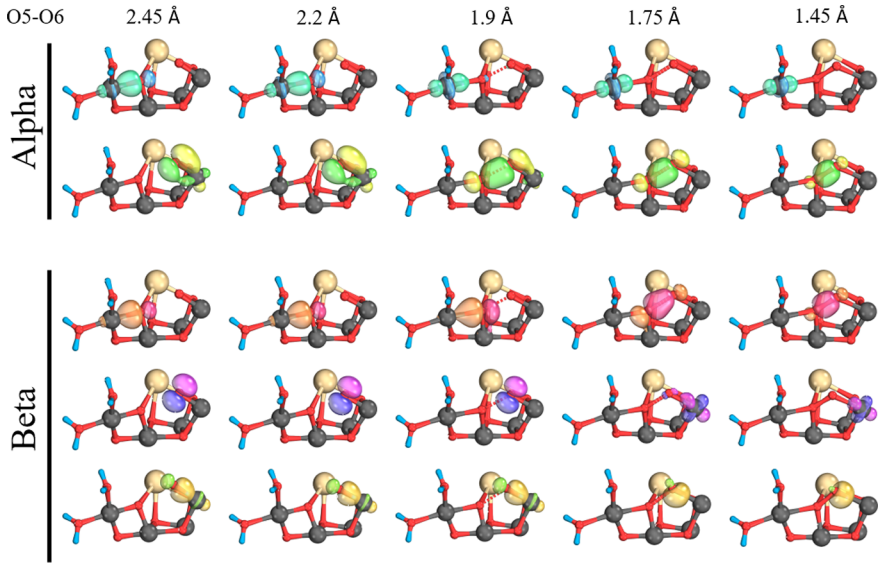

Figure 5. Intrinsic bond orbital (IBO) analysis of the M_s = 3.5 state oxo–oxo form. IBOs are given at the indicated O5–O6 separations showing α and β spin evolution.

https://doi.org/10.1021/acs.jpclett.3c03026
J. Phys. Chem. Lett. 2024, 15, 499−506

coupling. For electron transfer between interacting spin systems it has been found that the relative orientation of the two spin centers can be important for electron transfer and that the strength of the coupling is proportional to the rate of electron transfer as described by Fermi's golden rule.[47−50] Observation of coupling between the OEC and the $Y_Z^{\bullet}$ residue may point toward the potential for efficient electron transfer between them. Furthermore, the relative strengths of the couplings between the various spin centers in the OEC with the $Y_Z^{\bullet}$ suggest the origin of the electron transfer pathway to be through either $[O5O6]^{3-}$ or Mn_1, or indeed through both, to the $Y_Z^{\bullet}$ residue. Identifying the nature of the electron transfer process between the OEC and $Y_Z^{\bullet}$ is crucial, as this is a key step in the transition between the S_3 and S_4 state.

The $S_3Y_Z^{\bullet}$ state is an intermediate S-state, and so far it has not been possible to isolate it, limiting the amount of experimental data for it. Nonetheless some data is available; for example, EPR detects a split signal when the S_3 or indeed S_{0-3} is illuminated by light of a specific wavelength. This has been attributed to the presence of a $Y_Z^{\bullet}$ radical.[51] The ground state spin between the S_3 and $S_3Y_Z^{\bullet}$ state intermediates differs; in the S_3 the calculated ground state spin for the oxo−hydroxo, $[O5O6]^{3-}$, and peroxo species are 3, 6, and 3, respectively, whereas in the $S_3Y_Z^{\bullet}$ state they were 3.5, 5.5, and 3.5, respectively. As such, EPR should be able to differentiate between them. To the best of the authors' knowledge, however, so far the ground state spin of the species in the $S_3Y_Z^{\bullet}$ state has not been determined. XFEL studies have shed some light on the sequence of events for the S_3 to S_0 state;[34,35] these suggest that the $Y_Z^{\bullet}$ is present until O6 disappears (suggesting O_2 formation), in line with the mechanism proposed here in which the peroxo species is oxidized to reduce the $Y_Z^{\bullet}$ radical forming superoxo, which would rapidly form molecular oxygen.

Both the $[O5O6]^{3-}$ species and the peroxo species presented here showed significant exchange coupling interactions between the $Y_Z^{\bullet}$ radical and the OEC through the shared spin of Mn_1 and [O5O6] shared spin. On the other hand the oxo−hydroxo species showed no exchange interaction agreeing well with previous S_2 state work.[38] The species differ by both the O5−O6 separation as well as the O6 protonation state and orbital orientations, as seen for the $[O5O6]^{3-}$ species where the O6 lone pair was found to point toward the $Y_Z^{\bullet}$ radical in the $S_3Y_Z^{\bullet}$ state but not in the S_3 state. For the $[O5O6]^{3-}$ species, antiferromagnetic coupling between the $Y_Z^{\bullet}$ radical and O5/O6 was observed along with weaker coupling between $Y_Z^{\bullet}$ and the Mn ions. Weaker couplings between Mn_1 and the remaining Mn ions, and reduced [O5O6]−Mn couplings when compared to the S_3 state, suggest that the $[O5O6]^{3-}$ species is relatively destabilized in the $S_3Y_Z^{\bullet}$ state compared to the S_3 state agreeing with the relative energetics of the BS states.

Similarly, for the peroxo species, large exchange couplings were observed between the $Y_Z^{\bullet}$ radical and the Mn ions, with particularly strong coupling observed with Mn_1. An additional IBO was observed to change significantly in the $S_3Y_Z^{\bullet}$ state, and two IBOs, both involving Mn_1 and O6, showed major differences in their behavior when compared to the S_3 state, further pointing toward long-range exchange coupling between the $Y_Z^{\bullet}$ radical and the OEC. This would suggest potential facilitation of electron transfer from OEC to $Y_Z^{\bullet}$ through the coupled [O5O6], Mn_1, and $Y_Z^{\bullet}$ spin centers.

Throughout the Kok cycle, Y_Z subsequentially removes electrons from the OEC, preparing the system for facile molecular oxygen evolution. As the O5−O6 bond is formed, increased exchange coupling between the $Y_Z^{\bullet}$ radical and the OEC has been shown to emerge. The presence of this exchange coupling between the OEC and $Y_Z^{\bullet}$ may suggest a mechanism through which removal of the final electron from the OEC is promoted. The removal of the final electron would aid to drive the catalytic cycle to completion by promoting the onward reaction of peroxo. Due to the more stable nature of peroxo, it is reasonable to assume that additional driving force would be highly beneficial to this particular oxidation step.

METHODS

The methods used are similar to those described previously.[5,6,43] All calculations were performed in ORCA 4.[52] Models were initially optimized using the B3LYP functional[53,54] in their HS oxidation states. The zeroth-order regular approximation (ZORA) Hamiltonian was applied to account for scalar relativistic effects[55−57] with the def2-SVP basis sets used for C and H atoms and the def2-TZVP basis set without f functions for all other atoms.[58] For the systems presented here the B3LYP functional was chosen as it has been shown to work well for systems of this size and for energetics and orbital analysis for the OEC[59] as well as other transition metal systems.[60] The chain of spheres (RIJCOSX) approximation was applied together with the decontracted general Weigend auxilary basis sets.[61−65] The conductor-like polarizable continuum model (CPCM) with a dielectric constant of ϵ = 8.0 was used throughout to model the protein environment,[66,67] along with the dispersion corrections proposed by Grimme with Becke−Johnson damping (D3BJ).[68,69] Tight SCF convergence criteria and increased integration grids (Grid6 and IntAcc 6 in the ORCA convention) were used throughout, and all terminal carbon atoms were constrained during optimizations.

Initial BS-DFT wave functions were calculated using ZORA versions of the def2-TZVP with removed f functions for all atoms, and used for potential energy surface calculations.[58] The initial BS guesses were obtained by use of the "flipspin" feature of ORCA.[70] Also, convergence of the correct BS and HS states was confirmed by examination of the calculated Mulliken spin populations for all calculations. Throughout the text, these BS states may be referred to as BS1 or BS4, for example, indicating a BS state with Mn_1 or Mn_4 flipped, respectively.

The potential energy surface was obtained using the geometry optimization method as described above. The BS ".gbw" file for the M_s state in question was initially read in, and the O5−O6 bond length was varied between 2.45 to 1.45 Å in 0.05 Å steps, where each point underwent full geometry optimization to produce the final potential energy surface. To investigate the relative energies of His190 and Y_Z protonated structures, a high-spin O5−O6 peroxo or high-spin O5 oxo−O6 oxo was optimized. The proton was then moved onto either His190 or Y_Z, and single point calculations were performed for various BS states. Intrinsic bond orbitals (IBOs) were produced using IboView with iboexp = 2 from the optimized PES wave functions.

All models were generated from the S_3 XFEL crystal structure (PDB: 6DHO)[9] and optimized in the $S_3Y_Z^{\bullet}$ state. Seven directly coordinated amino acids are included in the models. Six are from the D1 protein chain (Asp170, Glu189,

https://doi.org/10.1021/acs.jpclett.3c03026
J. Phys. Chem. Lett. 2024, 15, 499−506

His332, Glu333, Asp342, Ala344, Tyr161 (Y_Z), and His190) and one from the CP43 protein chain (Glu354). The second sphere His337 residue was included along with the partial backbone of Ser169 (Figure S2). Terminal carbon atoms were constrained in all calculations. The directly coordinated water molecules W1−W4 as well as 11 crystallographic water molecules were also included. All oxygen bridges O1−O5 were in their fully deprotonated form (O^{2-}); O6 was $^{-}$OH for the O5 oxo−O6 hydroxo models, and was O^{2-} otherwise. W1, W3, and W4 were fully protonated, and W2 was $^{-}$OH for the O5 oxo−O6 hydroxo models, and fully protonated otherwise.

■ ASSOCIATED CONTENT

Supporting Information

The Supporting Information is available free of charge at https://pubs.acs.org/doi/10.1021/acs.jpclett.3c03026.

Supplementary IBOs and structural illustration (PDF)

■ AUTHOR INFORMATION

Corresponding Author

Thomas Malcomson − *School of Biosciences, Cardiff University, Cardiff CF10 3AX, United Kingdom;* orcid.org/0000-0002-1401-7976; Email: malcomsonT@cardiff.ac.uk

Authors

Felix Rummel − *Department of Chemistry, School of Natural Sciences, The University of Manchester, Manchester M13 9PL, United Kingdom*

Maxim Barchenko − *Department of Chemistry, School of Natural Sciences, The University of Manchester, Manchester M13 9PL, United Kingdom*

Patrick J. O'Malley − *Department of Chemistry, School of Natural Sciences, The University of Manchester, Manchester M13 9PL, United Kingdom;* orcid.org/0000-0002-1933-3740

Complete contact information is available at: https://pubs.acs.org/10.1021/acs.jpclett.3c03026

Notes

The authors declare no competing financial interest.

■ ACKNOWLEDGMENTS

F.R. acknowledges support from the UK BBSRC Doctoral Training Partnership (DTP) program. This research was supported with a grant from the Leverhulme Trust (RPG-2020-003). The authors would like to acknowledge the assistance given by Research IT and the use of the Computational Shared Facility at the University of Manchester.

■ REFERENCES

(1) Dau, H.; Zaharieva, I.; Haumann, M. Recent Developments in Research on Water Oxidation by Photosystem II. *Curr. Opin. Chem. Biol.* **2012**, *16*, 3−10.

(2) McEvoy, J. P.; Brudvig, G. W. Water-Splitting Chemistry of Photosystem II. *Chem. Rev.* **2006**, *106*, 4455−4483.

(3) Barber, J. Photosystem II: the Water Splitting Enzyme of Photosynthesis and the Origin of Oxygen in our Atmosphere. *Q. Rev. Biophys.* **2016**, *49*, No. e14.

(4) Perez-Navarro, M.; Neese, F.; Lubitz, W.; Pantazis, D. A; Cox, N. Recent Developments in Biological Water Oxidation. *Curr. Opin. Chem. Biol.* **2016**, *31*, 113−119.

(5) Rummel, F.; O'Malley, P. J. How Nature Makes O_2: an Electronic Level Mechanism for Water Oxidation in Photosynthesis. *J. Phys. Chem. B* **2022**, *126*, 8214−8221.

(6) Corry, T. A.; O'Malley, P. J. Evidence of O−O Bond Formation in the Final Metastable S_3 State of Nature's Water Oxidizing Complex Implying a Novel Mechanism of Water Oxidation. *J. Phys. Chem. Lett.* **2018**, *9*, 6269−6274.

(7) Corry, T. A.; O'Malley, P. J. S_3 State Models of Nature's Water Oxidizing Complex: Analysis of Bonding and Magnetic Exchange Pathways, Assessment of Experimental Electron Paramagnetic Resonance Data, and Implications for the Water Oxidation Mechanism. *J. Phys. Chem. B* **2021**, *125*, 10097−10107.

(8) Corry, T. A.; O'Malley, P. J. Electronic−Level View of O−O Bond Formation in Nature's Water Oxidizing Complex. *J. Phys. Chem. Lett.* **2020**, *11*, 4221−4225.

(9) Kern, J.; Chatterjee, R.; Young, I. D.; Fuller, F. D.; Lassalle, L.; Ibrahim, M.; Gul, S.; Fransson, T.; Brewster, A. S.; Alonso-Mori, R.; Hussein, R.; Zhang, M.; Douthit, L.; de Lichtenberg, C.; Cheah, M. H.; Shevela, D.; Wersig, J.; Seuffert, I.; Sokaras, D.; Pastor, E.; Weninger, C.; Kroll, T.; Sierra, R. G.; Aller, P.; Butryn, A.; Orville, A. M.; Liang, M.; Batyuk, A.; Koglin, J. E.; Carbajo, S.; Boutet, S.; Moriarty, N. W.; Holton, J. M.; Dobbek, H.; Adams, P. D.; Bergmann, U.; Sauter, N. K.; Zouni, A.; Messinger, J.; Yano, J.; Yachandra, V. K. Structures of the Intermediates of Kok's Photosynthetic Water Oxidation Clock. *Nature* **2018**, *563*, 421−425.

(10) Suga, M.; Akita, F.; Yamashita, K.; Nakajima, Y.; Ueno, G.; Li, H.; Yamane, T.; Hirata, K.; Umena, Y.; Yonekura, S.; Yu, L.-J.; Murakami, H.; Nomura, T.; Kimura, T.; Kubo, M.; Baba, S.; Kumasaka, T.; Tono, K.; Yabashi, M.; Isobe, H.; Yamaguchi, K.; Yamamoto, M.; Ago, H.; Shen, J.-R. An Oxyl/Oxo Mechanism for Oxygen-Oxygen Coupling in PSII Revealed by an X-Ray Free-Electron Laser. *Science* **2019**, *366*, 334−338.

(11) Suga, M.; Akita, F.; Sugahara, M.; Kubo, M.; Nakajima, Y.; Nakane, T.; Yamashita, K.; Umena, Y.; Nakabayashi, M.; Yamane, T.; Nakano, T.; Suzuki, M.; Masuda, T.; Inoue, S.; Kimura, T.; Nomura, T.; Yonekura, S.; Yu, L.-J.; Sakamoto, T.; Motomura, T.; Chen, J.-H.; Kato, Y.; Noguchi, T.; Tono, K.; Joti, Y.; Kameshima, T.; Hatsui, T.; Nango, E.; Tanaka, R.; Naitow, H.; Matsuura, Y.; Yamashita, A.; Yamamoto, M.; Nureki, O.; Yabashi, M.; Ishikawa, T.; Iwata, S.; Shen, J.-R. Light-Induced Structural Changes and the Site of O = O Bond Formation in PSII Caught by XFEL. *Nature* **2017**, *543*, 131−135.

(12) Ibrahim, M.; Fransson, T.; Chatterjee, R.; Cheah, M. H.; Hussein, R.; Lassalle, L.; Sutherlin, K. D.; Young, I. D.; Fuller, F. D.; Gul, S.; Kim, I.-S.; Simon, P. S.; de Lichtenberg, C.; Chernev, P.; Bogacz, I.; Pham, C. C.; Orville, A. M.; Saichek, N.; Northen, T.; Batyuk, A.; Carbajo, S.; Alonso-Mori, R.; Tono, K.; Owada, S.; Bhowmick, A.; Bolotovsky, R.; Mendez, D.; Moriarty, N. W.; Holton, J. M.; Dobbek, H.; Brewster, A. S.; Adams, P. D.; Sauter, N. K.; Bergmann, U.; Zouni, A.; Messinger, J.; Kern, J.; Yachandra, V. K.; Yano, J. Untangling the Sequence of Events During the S_2; S_3 Transition in Photosystem II and Implications for the Water Oxidation Mechanism. *Proc. Natl. Acad. Sci. U. S. A.* **2020**, *117*, 12624−12635.

(13) Sproviero, E. M.; Gascón, J. A.; McEvoy, J. P.; Brudvig, G. W.; Batista, V. S. QM/MM Models of the O_2-Evolving Complex of Photosystem II. *J. Chem. Theory Comput.* **2006**, *2*, 1119−1134.

(14) Chabi, S.; Papadantonakis, K. M.; Lewis, N. S.; Freund, M. S. Membranes for Artifical Photosynthesis. *Energy Envirn. Sci.* **2017**, *10*, 1320−1338.

(15) Cox, N.; Pantazis, D. A.; Neese, F.; Lubitz, W. Artifical Photosynthesis: Understanding Water Splitting in Nature. *Interface Focus* **2015**, *5*, 20150009.

(16) Faunce, T. A.; Lubitz, W.; Rutherford, A. W.; MacFarlane, D.; Moore, G. F.; Yang, P.; Nocera, D. G.; Moore, T. A.; Gregory, D. H.; Fukuzumi, S.; Yoon, K. B.; Armstrong, F. A.; Wasielewski, M. R.; Styring, S. Energy and Environment Policy Case for a Global Project on Artificial Photosynthesis. *Energy Envirn. Sci.* **2013**, *6*, 695−698.

(17) Gratzel, M. Solar Energy Conversion by Dye-Sensitised Photovoltaic Cells. *Inorg. Chem.* **2005**, *44*, 6841−6851.

(18) McKone, J. R.; Crans, D. C.; Martin, C.; Turner, J.; Duggal, A. R.; Gray, H. R. Translational Science for Energy and Beyond. *Inorg. Chem.* **2016**, *55*, 9131−9143.
(19) Nocera, D. G. The Artifical Leaf. *Acc. Chem. Res.* **2012**, *45*, 767−776.
(20) Nocera, D. G. Solar Fuels and Solar Chemicals Industry. *Acc. Chem. Res.* **2017**, *50*, 616−619.
(21) Suga, M.; Akita, F.; Sugahara, M.; Kubo, M.; Nakajima, Y.; Nakane, T.; Yamashita, K.; Umena, Y.; Nakabayashi, M.; Yamane, T.; Nakano, T.; Suzuki, M.; Masuda, T.; Inoue, S.; Kimura, T.; Nomura, T.; Yonekura, S.; Yu, L.-J.; Sakamoto, T.; Motomura, T.; Chen, J.-H.; Kato, Y.; Noguchi, T.; Tono, K.; Joti, Y.; Kameshima, T.; Hatsui, T.; Nango, E.; Tanaka, R.; Naitow, H.; Matsuura, Y.; Yamashita, A.; Yamamoto, M.; Nureki, O.; Yabashi, M.; Ishikawa, T.; Iwata, S.; Shen, J.-R. Light-Induced Structural Changes and the Site of O = O Bond Formation in PSII Caught by XFEL. *Nature* **2017**, *543*, 131−135.
(22) Pantazis, D. A. The S_3 State of the Oxygen-Evolving Complex: Overview of Spectroscopy and XFEL Crystallography with a Critical Evaluation of Early-Onset Models for O−O Bond Formation. *Inorganics* **2019**, *7*, 55−85.
(23) Messinger, J.; Badger, M.; Wydrzynski, T. Detection of One Slowly Exchanging Substrate Water Molecule in the S_3 State of Photosystem II. *Proc. Natl. Acad. Sci. U.S.A.* **1995**, *92*, 3209−3219.
(24) Cox, N.; Retegan, M.; Neese, F.; Pantazis, D. A.; Boussac, A.; Lubitz, W. Electronic Structure of the Oxygen-Evolving Complex in Photosystem II Prior to O-O Bond Formation. *Science* **2014**, *345*, 804−808.
(25) Kern, J.; Chatterjee, R.; Young, I. D.; Fuller, F. D.; Lassalle, L.; Ibrahim, M.; Gul, S.; Fransson, T.; Brewster, A. S.; Alonso-Mori, R.; Hussein, R.; Zhang, M.; Douthit, L.; de Lichtenberg, C.; Cheah, M. H.; Shevela, D.; Wersig, J.; Seuffert, I.; Sokaras, D.; Pastor, E.; Weninger, C.; Kroll, T.; Sierra, R. G.; Aller, P.; Butryn, A.; Orville, A. M.; Liang, M.; Batyuk, A.; Koglin, J. E.; Carbajo, S.; Boutet, S.; Moriarty, N. W.; Holton, J. M.; Dobbek, H.; Adams, P. D.; Bergmann, U.; Sauter, N. K.; Zouni, A.; Messinger, J.; Yano, J.; Yachandra, V. K. Structures of the Intermediates of Kok's Photosynthetic Water Oxidation Clock. *Nature* **2018**, *563*, 421−425.
(26) Cox, N.; Retegan, M.; Neese, F.; Pantazis, D. A.; Boussac, A.; Lubitz, W. Electronic Structure of the Oxygen-Evolving Complex in Photosystem II Prior to O-O Bond Formation. *Science* **2014**, *345*, 804−808.
(27) Krewald, V.; Retegan, M.; Cox, N.; Messinger, J.; Lubitz, W.; De Beer, S.; Neese, F.; Pantazis, D. A. Metal Oxidation States in Biological Water Splitting. *Chem. Sci.* **2015**, *6*, 1676−1695.
(28) Krewald, V.; Retegan, M.; Neese, F.; Lubitz, W.; Pantazis, D. A.; Cox, N. Spin State as a Marker for the Structural Evolution of Nature's Water Splitting Catalyst. *Inorg. Chem.* **2016**, *55*, 488−501.
(29) Zaharieva, I.; Chernev, P.; Berggren, G.; Anderlund, M.; Styring, S.; Dau, H.; Haumann, M. Room-Temperature Energy-Sampling Kβ X-ray Emission Spectroscopy of the Mn_4Ca Complex of Photosynthesis Reveals Three Manganese-Centered Oxidation Steps and Suggests a Coordination Change Prior to O_2 Formation. *Biochemistry* **2016**, *55*, 4197−4211.
(30) Zaharieva, I.; Dau, H.; Haumann, M. Room-Temperature Energy-Sampling Kβ X-ray Emission Spectroscopy of the Mn_4Ca Complex of Photosynthesis Reveals Three Manganese-Centered Oxidation Steps and Suggests a Coordination Change Prior to O_2 Formation. *Biochemistry* **2016**, *55*, 6996−7004.
(31) Haumann, M.; Liebisch, P.; Müller, C.; Barra, M.; Grabolle, M.; Dau, H. Photosynthetic O_2 Formation Tracked by Time-Resolved X-Ray Experiments. *Science* **2005**, *310*, 1019−1021.
(32) Haumann, M.; Grundmeier, A.; Zaharieva, I.; Dau, H. Photosynthetic Water Oxidation at Elevated Dioxygen Partial Pressure Monitored by Time-Resolved X-Ray Absorption Measures. *Proc. Natl. Acad. Sci. U.S.A.* **2008**, *105*, 17384−17389.
(33) Kolling, D. R. J.; Brown, T. S.; Ananyev, G.; Dismukes, G. C. Photosynthetic Oxygen Evolution is Not Reversed at High Oxygen Pressures: Mechanistic Consequences for the Water-Oxidising Complex. *Biochemistry* **2009**, *48*, 1381−1389.
(34) Greife, P.; Schönborn, M.; Capone, M.; Assunção, R.; Narzi, D.; Guidoni, L.; Dau, H. The Electron−Proton Bottleneck of Photosynthetic Oxygen Evolution. *Nature* **2023**, *617*, 623−628.
(35) Bhowmick, A.; Hussein, R.; Bogacz, I.; Simon, P. S.; Ibrahim, M.; Chatterjee, R.; Doyle, M. D.; Cheah, M. H.; Fransson, T.; Chernev, P.; Kim, I.-S.; Makita, H.; Dasgupta, M.; Kaminsky, C. J.; Zhang, M.; Gätcke, J.; Haupt, S.; Nangca, I. I.; Keable, S. M.; Aydin, A. O.; Tono, K.; Owada, S.; Gee, L. B.; Fuller, F. D.; Batyuk, A.; Alonso-Mori, R.; Holton, J. M.; Paley, D. W.; Moriarty, N. W.; Mamedov, F.; Adams, P. D.; Brewster, A. S.; Dobbek, H.; Sauter, N. K.; Bergmann, U.; Zouni, A.; Messinger, J.; Kern, J.; Yano, J.; Yachandra, V. K. Structural Evidence for Intermediates During O_2 Formation in Photosystem II. *Nature* **2023**, *617*, 629−636.
(36) Cox, N.; Pantazis, D. A.; Lubitz, W. Current Understanding of the Mechanism of Water Oxidation in Photosystem II and Its Relation to XFEL Data. *Annu. Rev. Biochem.* **2020**, *89*, 795−820.
(37) Pushkar, Y.; Davis, K. M.; Palenik, M. C. Model of the Oxygen Evolving Complex which is Highly Predisposed to O-O Bond Formation. *J. Phys. Chem. Lett.* **2018**, *9*, 3525−3531.
(38) Retegan, M.; Cox, N.; Lubitz, W.; Neese, F.; Pantazis, D. A. The First Tyrosyl Radical Intermediate Formed in the S_2−S_3 transition of photosystem II. *Phys. Chem. Chem. Phys.* **2014**, *16*, 11901−11910.
(39) Bürger, K.-S.; Chaudhuri, P.; Wieghardt, K.; Nuber, B. Intramolecular Long-Range Exchange Coupling in Dinuclear Copper-(II) Complexes with Cu Cu Separations Greater than 10Å. *Chem.—Eur. J.* **1995**, *1*, 583−593.
(40) Liu, Y.; Villamena, F. A.; Rockenbauer, A.; Song, Y.; Zweier, J. L. Structural Factors Controlling the Spin−Spin Exchange Coupling: EPR Spectroscopic Studies of Highly Asymmetric Trityl−Nitroxide Biradicals. *J. Am. Chem. Soc.* **2013**, *135*, 2350−2356.
(41) Stanford, M. W.; Knight, F. R.; Athukorala Arachchige, K. S.; Sanz Camacho, P.; Ashbrook, S. E.; Bühl, M.; Slawin, A. M. Z.; Woollins, J. D. Probing Interactions Through Space Using Spin−Spin Coupling. *Dalton Trans* **2014**, *43*, 6548−6560.
(42) Curtiss, L. A.; Naleway, C. A.; Miller, J. R. Superexchange Pathway Calculation of Long-Distance Electronic Coupling in $H_2C(CH_2)_{m-2}CH_2$ Chains. *Chem. Phys.* **1993**, *176*, 387−405.
(43) Corry, T. A.; Rummel, F.; O'Malley, P. J. Bonding and Magnetic Exchange Pathways in Nature's Water-Oxidizing Complex. *J. Phys. Chem. B* **2021**, *125*, 7147−7154.
(44) Di Valentin, M.; Tait, C. E.; Salvadori, E.; Orian, L.; Polimeno, A.; Carbonera, D. Evidence for Water-Mediated Triplet−Triplet Energy Transfer in the Photoprotective Site of the Peridinin−Chlorophyll A−Protein. *Biochimica et Biophysica Acta (BBA) - Bioenergetics* **2014**, *1837*, 85−97.
(45) Lin, J.; Balabin, I. A.; Beratan, D. N. The Nature of Aqueous Tunneling Pathways Between Electron-Transfer Proteins. *Science* **2005**, *310*, 1311−1313.
(46) Curutchet, C.; Voityuk, A. A. Distance Dependence of Triplet Energy Transfer in Water and Organic Solvents: A QM/MD Study. *J. Phys. Chem. C* **2012**, *116*, 22179−22185.
(47) Devault, D. *Quantum Mechanical Tunneling in Biological Systems*; Cambridge University Press: Cambridge, 1984.
(48) Newton, M. D.; Sutin, N. Electron Transfer Reactions in Condensed Phases. *Annu. Rev. Phys. Chem.* **1984**, *35*, 437−480.
(49) Marcus, R.; Sutin, N. Electron Transfers in Chemistry and Biology. *Biochimica et Biophysica Acta (BBA) - Reviews on Bioenergetics* **1985**, *811*, 265−322.
(50) Lukas, A. S.; Bushard, P. J.; Wasielewski, M. R. Electron Transfer Involving Nonbonded Superexchange Interactions in Rigid Donor-Acceptor Arrays. *J. Phys. Chem. A* **2002**, *106*, 2074−2082.
(51) Su, J.-H.; Havelius, K. G. V.; Ho, F. M.; Han, G.; Mamedov, F.; Styring, S. Formation Spectra of the EPR Split Signals from the S0, S1, and S3 States in Photosystem II Induced by Monochromatic Light at 5 K. *Biochemistry* **2007**, *46*, 10703−10712.
(52) Neese, F. Software Update: the ORCA Program System, Version 4.0. *WIREs Computational Molecular Science* **2018**, *8*, No. e1327.

https://doi.org/10.1021/acs.jpclett.3c03026
J. Phys. Chem. Lett. 2024, 15, 499−506

(53) Lee, C.; Yang, W.; Parr, R. G. Development of the Colle-Salvetti Correlation-Energy Formula into a Functional of the Electron Density. *Phys. Rev. B* **1988**, *37*, 785−789.
(54) Becke, A. D. A. New Mixing of Hartree−Fock and Local Density-Functional Theories. *J. Chem. Phys.* **1993**, *98*, 1372−1377.
(55) Lenthe, E. v.; Baerends, E. J.; Snijders, J. G. Relativistic Regular Two-Component Hamiltonians. *J. Chem. Phys.* **1993**, *99*, 4597−4610.
(56) van Lenthe, E.; Baerends, E. J.; Snijders, J. G. Relativistic Total Energy Using Regular Approximations. *J. Chem. Phys.* **1994**, *101*, 9783−9792.
(57) van Wüllen, C. Molecular Density Functional Calculations in the Regular Relativistic Approximation: Method, Application to Coinage Metal Diatomics, Hydrides, Fluorides and Chlorides, and Comparison with First-Order Relativistic Calculations. *J. Chem. Phys.* **1998**, *109*, 392−399.
(58) Weigend, F.; Ahlrichs, R. Balanced Basis Sets of Split Valence, Triple Zeta Valence and Quadruple Zeta Valence Quality for H to Rn: Design and Assessment of Accuracy. *Phys. Chem. Chem. Phys.* **2005**, *7*, 3297−3305.
(59) Siegbahn, P. E. M. Nucleophilic Water Attack is not a Possible Mechanism for O−O Bond Formation in Photosystem II. *Proc. Natl. Acad. Sci. U. S. A.* **2017**, *114*, 4966−4968.
(60) Altun, A.; Breidung, J.; Neese, F.; Thiel, W. Correlated Ab Initio and Density Functional Studies on H2 Activation by FeO^+. *J. Chem. Theory Comput.* **2014**, *10*, 3807−3820.
(61) Eichkorn, K.; Treutler, O.; Öhm, H.; Häser, M.; Ahlrichs, R. Auxiliary Basis Sets to Approximate Coulomb Potentials. *Chem. Phys. Lett.* **1995**, *240*, 283−290.
(62) Eichkorn, K.; Weigend, F.; Treutler, O.; Ahlrichs, R. Auxiliary Basis Sets for Main Row Atoms and Transition Metals and Their use to Approximate Coulomb Potentials. *Theor. Chem. Acc.* **1997**, *97*, 119−124.
(63) Weigend, F. Accurate Coulomb-Fitting Basis Sets for H to Rn. *Phys. Chem. Chem. Phys.* **2006**, *8*, 1057−1065.
(64) Staroverov, V. N.; Scuseria, G. E.; Tao, J.; Perdew, J. P. Comparative Assessment of a New Nonempirical Density Functional: Molecules and Hydrogen-Bonded Complexes. *J. Chem. Phys.* **2003**, *119*, 12129−12137.
(65) Neese, F.; Wennmohs, F.; Hansen, A.; Becker, U. Efficient, Approximate and Parallel Hartree−Fock and Hybrid DFT Calculations. A 'Chain-of-Spheres' Algorithm for the Hartree−Fock Exchange. *Chem. Phys.* **2009**, *356*, 98−109.
(66) Cox, N.; Retegan, M.; Neese, F.; Pantazis, D. A.; Boussac, A.; Lubitz, W. Electronic Structure of the Oxygen-Evolving Complex in Photosystem II Prior to O-O Bond Formation. *Science* **2014**, *345*, 804−808.
(67) Pantazis, D. A.; Ames, W.; Cox, N.; Lubitz, W.; Neese, F. Two Interconvertible Structures that Explain the Spectroscopic Properties of the Oxygen-Evolving Complex of Photosystem II in the S_2 State. *Angew. Chem., Int. Ed.* **2012**, *51*, 9935−9940.
(68) Grimme, S.; Antony, J.; Ehrlich, S.; Krieg, H. A Consistent and Accurate Ab Initio Parametrization of Density Functional Dispersion Correction (DFT-D) for the 94 Elements H-Pu. *J. Chem. Phys.* **2010**, *132*, 154104.
(69) Grimme, S.; Ehrlich, S.; Goerigk, L. Effect of the Damping Function in Dispersion Corrected Density Functional Theory. *J. Comput. Chem.* **2011**, *32*, 1456−1465.
(70) Neese, F. The ORCA Program System. *WIREs Computational Molecular Science* **2012**, *2*, 73−78.

https://doi.org/10.1021/acs.jpclett.3c03026
J. Phys. Chem. Lett. 2024, 15, 499−506